The solubility of tugarinovite (MoO2) in H2O at elevated temperatures and pressures

Pritam Saha, Alan J. Anderson, Thomas Lee, Matthias Klemm

Angaben zur Veröffentlichung / Publication details:

Saha, Pritam, Alan J. Anderson, Thomas Lee, and Matthias Klemm. 2017. "The solubility of tugarinovite (MoO2) in H2O at elevated temperatures and pressures." *Geofluids* 2017: 5459639. https://doi.org/10.1155/2017/5459639.

Hindawi
Geofluids
Volume 2017, Article ID 5459639, 12 pages
https://doi.org/10.1155/2017/5459639

Research Article

The Solubility of Tugarinovite (MoO_2) in H_2O at Elevated Temperatures and Pressures

Pritam Saha,[1] Alan J. Anderson,[1] Thomas Lee,[1] and Matthias Klemm[2]

[1]*Department of Earth Sciences, St. Francis Xavier University, Antigonish, NS, Canada B2G 2W5*
[2]*Experimentalphysik II, Institut für Physik, Universität Augsburg, 86135 Augsburg, Germany*

Correspondence should be addressed to Pritam Saha; saha_pritam@ymail.com

Received 12 September 2017; Accepted 21 November 2017; Published 18 December 2017

Academic Editor: Andri Stefansson

The solubility of tugarinovite (MoO_2) in pure water was investigated at temperatures between 400 and 800°C and at pressures ranging between 95 and 480 MPa by using in situ synchrotron X-ray fluorescence (SXRF) to separately analyze high temperature aqueous solutions in a hydrothermal diamond anvil cell (HDAC). The concentration of molybdenum in the fluid at 400 and 500°C was below detection; however, at temperatures between 600 and 800°C, the solubility of tugarinovite increased with increasing temperature by two orders of magnitude. The molybdenum concentration at 600°C and 800°C is 44 ppm and 658 ppm, respectively. The results complement the data of Kudrin (1985) and provide the first measurement of MoO_2 solubility at pressure and temperature conditions comparable to intrusion-related Mo deposit formation. The data are also relevant to the study of water chemistry and corrosion product transport in supercritical-water-cooled reactors, where Mo-bearing steel alloys interact with aqueous solutions at temperatures greater than 600°C. The application of in situ SXRF to solubility measurements of sparingly soluble minerals is recommended because it circumvents analytical uncertainties inherent in determinations obtained by quenching and weight loss measurements.

1. Introduction

Metal solubility data over a wide range of temperatures and pressures are fundamental for a quantitative modelling of the metal transport by hydrothermal fluids in the Earth crust and in various industrial processes. Molybdenum in magmatic ore deposits is transported and deposited by high temperature aqueous fluids exsolved from a cooling magma. Although the solubility of MoO_3 (molybdite) has been experimentally investigated over a wide range of P-T-X conditions by many workers [1–7], comparatively few studies have examined the solubility of MoO_2 (tugarinovite) [8–10]. In the absence of sulfur, MoO_2, rather than MoO_3, would be the stable oxide at the temperatures and fo_2 conditions typical for Mo ore formation [4, 7, 11, 12].

The addition of molybdenum as an alloying element increases the tensile strength and chemical durability of steel used in jet engines, gas turbines, and power generation reactors [13, 14]. Molybdenum-bearing high strength steel alloys are among the candidate materials considered for use in the construction of the next generation of supercritical-water-cooled reactors (SCWR) [15, 16]. For example, the Generation-IV SCWR, which is designed to function at temperatures up to 625°C and pressures ranging from 25 to 30 MPa [15], is one of the six reactor design concepts developed to meet the need for an energy efficient advanced reactor [17]. An important challenge in the design and successful deployment of a SCWR is controlling water chemistry under conditions of high temperature and pressure [15, 18–21]. Hence, knowledge of the solubility of metal oxides produced at the steel-supercritical water interface is important for predicting corrosion and corrosion product transport within the reactor.

To this end, we present in situ synchrotron X-ray fluorescence (SXRF) analyses of supercritical aqueous fluids in equilibrium with synthetic MoO_2 in a modified Bassett-type hydrothermal diamond anvil cell (for design details of a Bassett-type HDAC see [22]). In situ analysis of the fluid at high temperature and pressure was employed in order to circumvent errors inherent in ex situ methods [23–26].

Our results complement the data of Kudrin [8] by providing solubility measurements at pressures and temperatures comparable to intrusion-related Mo ore formation and at the anticipated operating temperature conditions of supercritical-water-cooled reactors.

2. Previous Studies on Molybdenum Oxide Solubility

Natural molybdenum oxides include molybdite (MoO_3) and tugarinovite (MoO_2). Most solubility studies have been conducted on MoO_3. Ivanova et al. [1] performed dissolution experiments in Ti-autoclaves at vapour saturation pressures at temperatures between 150 and 300°C. The aqueous solutions, which were analyzed colorimetrically after quenching to room temperature, contained between 770 and 1390 ppm Mo. Gong et al. [2] used cold-seal pressure vessels to measure the solubility of MoO_3 at 417°C at pressures between 29 and 150 MPa. They showed that, at the studied P-T conditions, the solution contained 3200 ppm Mo. In both of these studies, however, neither pH nor oxygen fugacity were constrained.

Ulrich and Mavrogenes [4] trapped solutions equilibrated with MoO_3 in synthetic quartz-hosted fluid inclusions at pressures of 200 MPa and temperatures ranging between 500 and 800°C. The pH was buffered using a muscovite, K-feldspar, and quartz assemblage and the oxygen fugacity was constrained using a Ni/NiO or Re/ReO_2 buffer. Analysis of the synthetic fluid inclusions by laser ablation inductively coupled plasma mass spectrometry (LA-ICP-MS) shows that the molybdenum concentration in pure H_2O increased with increasing temperature from 380 to 8155 ppm. X-ray absorption near-edge structure (XANES) spectra obtained from synthetic fluid inclusions at the temperature of liquid-vapour homogenization suggest that the dominant Mo species is H_2MoO_4.

Meredith et al. [5] used synchrotron X-ray fluorescence to measure the solubility of MoO_3 in oxygenated water in a hydrothermal diamond anvil cell. The concentration of Mo in solution ranged from 3995 ± 13 ppm at 400°C and 44 MPa to 8663 ± 59 ppm at 500°C and 113 MPa.

Dadze et al. [6] determined the solubility of crystalline MoO_3 in aqueous solutions of $HClO_4$ at 300°C and 10 MPa. They suggested that the acidity of the solution was a determining factor controlling the solubility of molybdenum trioxide under hydrothermal conditions and assumed that monomeric forms $H_2MoO_4^0$, $HMoO_4^-$, and MoO_4^{2-} are produced by the dissolution of MoO_3. Rempel et al. [3] studied the solubility of molybdenum trioxide in water vapour at 300, 320, and 360°C and 3.9–15.4 MPa. They reported Mo concentrations of 17.9, 23.5, and 28.7 ppm at 300, 320, and 360°C, respectively, and concluded that the predominant species is a monomeric hydrated complex of the form $MoO_3 \cdot nH_2O(g)$. Hurtig and Williams-Jones [7] measured the solubility of MoO_3 in HCl-bearing water vapour and vapour-like aqueous fluids having a density between 0.005 and 0.343 g/cm^3 at temperatures between 300 and 500°C and 1.3–42.5 MPa. They suggested that, at 400°C and 20 MPa, the major molybdenum-bearing species in the low density aqueous solutions is $MoO_3(H_2O)_8$. They also noted that the hydration number of the dominant species decreases as the temperature increases. The concentration of molybdenum in the quenched experimental condensates ranged from 3 to 481 ppm. Titanium autoclaves were used in the experiments by Rempel et al. (2006); Dadze et al. (2014) and Hurtig and Williams-Jones (2014). Figure 1 shows MoO_3 solubility as a function of temperature reported in previous studies.

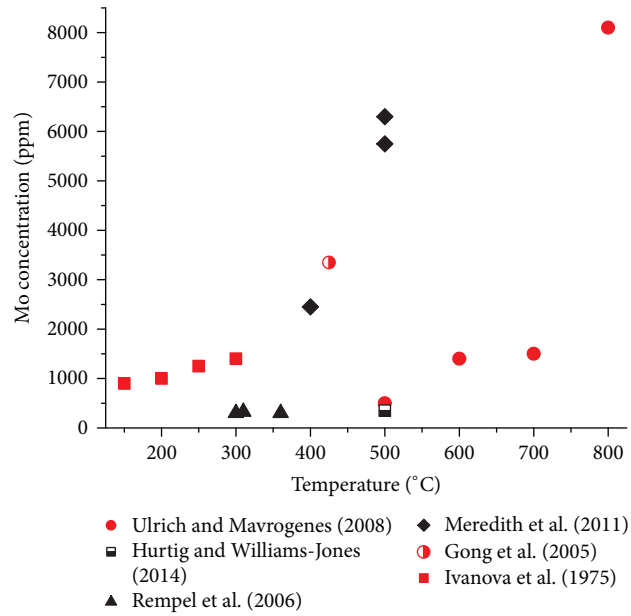

FIGURE 1: MoO_3 solubility versus temperature from previous studies. Pressures reported are 44–113 MPa (Meredith et al. 2011), 200 MPa (Ulrich and Mavrogenes 2008), 29–150 MPa (Gong et al. 2005), 1.3–42.5 MPa (Hurtig and Williams-Jones 2014), and 3.9–15.4 MPa (Rempel et al. 2006). Red symbols designate MoO_3 solubility in pure water.

Comparatively few data are available on the solubility of MoO_2 [8–10]. This is due to problems of measuring the solubility of sparingly soluble minerals under conditions of extreme temperature and pressure. Kudrin [8] determined the solubility of tugarinovite (MoO_2) in water and aqueous solutions of HCl, NaOH, and KOH at temperatures between 250 and 450°C and at pressures between 9 MPa and 100 MPa. He showed that the concentration of Mo in pure water increases with increasing temperature from 0.01 ppm at 300°C to 25 ppm at 450°C. The experiments were conducted using titanium autoclaves while the redox conditions were controlled using Ni-NiO, Cu-Cu_2O, or Fe_3O_4-Fe_2O_3 buffers. Kudrin suggested that various Mo (VI) hydroxy complexes are the predominant species of molybdenum in the solution. Cao [10] studied MoO_2 solubility in NaCl solution from 300 to 450°C using a chrome lined vessel and the solubility ranges from 5 to 315 ppm. He showed that, in these solutions, both Mo (V) and Mo (VI) can exist stably at high temperatures in the form of $HMoO_4^-$, $NaHMoO_4^0$, and $Na_2MoO_4^2$.

Table 1: X-ray diffraction data for synthetic MoO_2 crystals used as starting material and tugarinovite (MoO_2).

Synthetic MoO_2 starting material			Tugarinovite (JCPDS: file number 32-671)				
Pos. [°2θ]	d (Å)	Intensity	h	k	l	d (Å)	Intensity
18.3801	4.827	2.05	$\bar{1}$	0	1	4.805	2
25.9998	3.427	100	$\bar{1}$	1	1	3.420	100
31.9055	2.805	0.84	1	0	1	2.813	4
36.7193	2.447	7.93	2	0	0	2.442	30
			1	1	1	2.437	30
36.9918	2.430	18.92	$\bar{2}$	1	1	2.426	70
37.3586	2.407	12.09	$\bar{2}$	0	2	2.403	35
41.3568	2.183	1.67	2	1	0	2.181	6
			0	2	1	2.171	2
41.8854	2.157	2.53	$\bar{2}$	1	2	2.156	5
49.5028	1.841	2.97	$\bar{3}$	0	1	1.841	11
53.0658	1.726	11.45	2	1	1	1.725	30

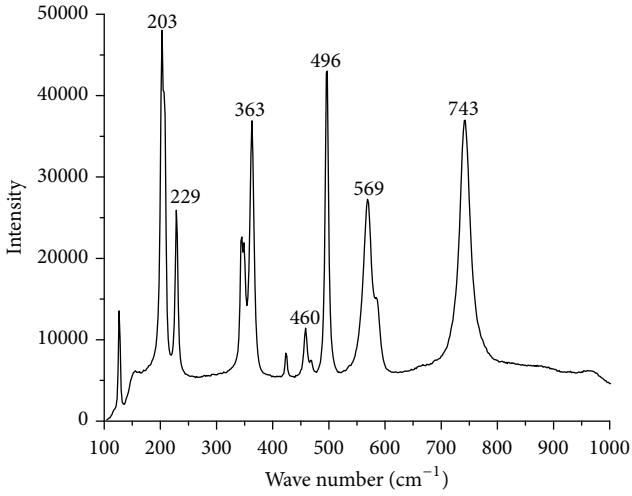

Figure 2: Raman spectrum of synthetic MoO_2 used as starting material.

3. Experimental Procedures

3.1. Synthesis and Characterization of Starting Materials. Crystals of synthetic MoO_2 were grown by chemical transport using $TeCl_4$ as a transport agent at the Institute of Physics, Augsburg University, Germany [27, 28]. X-ray powder diffraction data collected from the starting material using CuKα radiation is compared to tugarinovite [29] in Table 1.

Raman spectra of the starting material, obtained using a Horiba Jobin-Yvon LabRam HR confocal instrument equipped with a 100 mW 532 nm Nd-YAG diode laser (Toptica Photonics) and a Synapse charge-coupled device (CCD; Horiba Jobin-Yvon) detector at St. Mary's University, Halifax, are shown in Figure 2. Frequency calibration was performed using a pure silica standard (521 cm^{-1}). Each Raman spectrum represents an average of two accumulations with 20-second acquisition times at 100% laser power. Raman shifts for synthetic material are in close agreement with previously published Raman spectra obtained from MoO_2 [11, 12, 30–32].

3.2. Hydrothermal Diamond Anvil Cell. A Bassett-type hydrothermal diamond anvil cell (HDAC) was modified so that an aqueous fluid in equilibrium with MoO_2 could be separately analyzed by microbeam synchrotron X-ray fluorescence. The sample chamber consisted of a cylindrical-shaped laser-milled recess in the culet face of the upper diamond anvil and the hole in a rhenium gasket that was pressed between the two diamond anvils (Figure 3). Optical profilometer measurements indicated that the recess in the diamond is 300 μm in diameter and 37 μm deep (Figure 4), and the hole in the rhenium gasket is 125 μm deep and 400 μm in diameter.

The diamond anvils were fitted into silicon nitride seats located at the center of two opposing stainless steel platens. The platens were then drawn together along three guide posts using tightening screws. Each silicon nitride seat was heated using platinum resistance wire while the temperature of the system was monitored using S-type (Platinum-Rhodium) thermocouples (Omega™) and controlled with a programmable temperature controller. The temperature of sample chamber was calibrated by observing the melting point of $NaNO_3$ (308°C), the alpha-beta phase transition of quartz (573°C), and the melting point of NaCl (801°C). The water density was determined from the observed liquid-vapour homogenization temperature and the pressure at a given temperature was calculated using the equation of state (EOS) of water [33–35]. The EOS of pure water is a good estimate of pressure because of the very low Mo concentration in the fluid at all temperatures and pressures measured.

The MoO_2 crystal resides on the culet face of the lower diamond anvil and within the Re gasket (Figure 3(a)). A horizontal X-ray microbeam passes through the fluid-filled recess in the diamond anvil above the Re gasket. This configuration ensures that the incident X-ray beam does

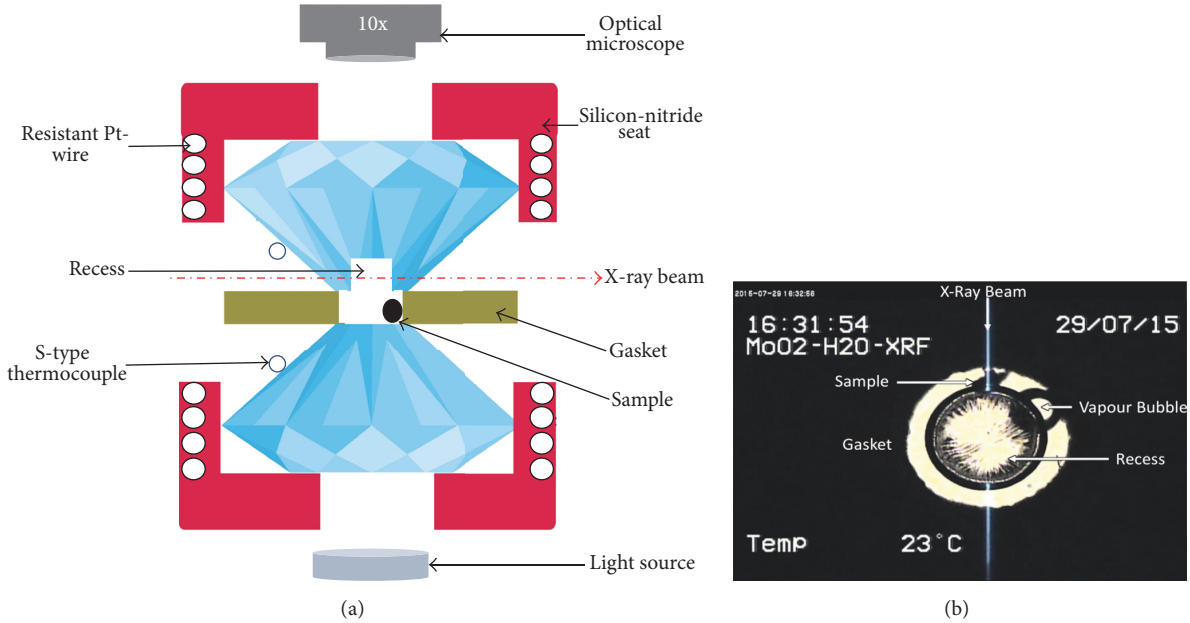

FIGURE 3: (a) The schematic diagram of the modified hydrothermal diamond anvil cell. The upper diamond anvil was recessed and the X-ray beam went through the recess. A rhenium gasket was squeezed by two diamond anvils together. A 10x objective microscope was placed on top of the HDAC to view the sample chamber in real time. (b) shows the sample chamber at room temperature. The MoO_2 sample, vapour bubble, and the recess of the upper diamond are visible. The sample chamber is surrounded by the rhenium gasket. The X-ray beam path (blue line) is also visible.

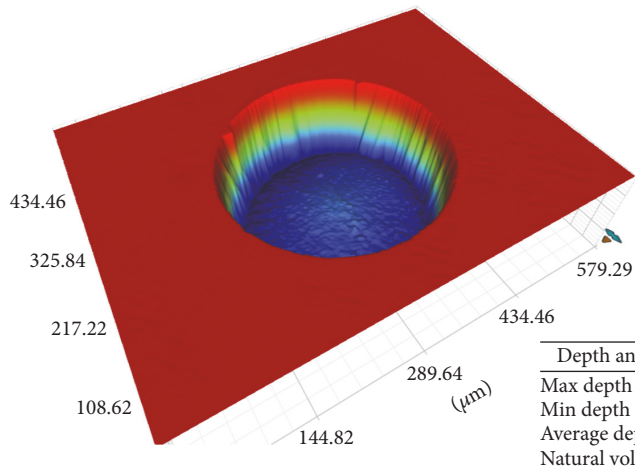

Depth and volume of the recess	
Max depth (μm)	46.41
Min depth (μm)	30.32
Average depth (μm)	37.19
Natural volume (cm^3)	$2.29E10^{-06}$

FIGURE 4: 3D profile of the culet face of the recessed diamond anvil. Inset shows the depth and volume of the recess. This 3D profile was prepared using an optical profilometer.

not interact with the MoO_2 crystal and that the detector is shielded from possible excitation of the crystal by scattered X-rays. Figure 3(b) is a photograph of the sample chamber as viewed through the diamond anvils showing the vapour bubble, the opaque MoO_2 crystal fragment in H_2O, and the path of the X-ray beam through the sample chamber.

The HDAC was purged with argon gas in order to prevent oxidation at high temperatures. Kapton film windows on the wall of the HDAC allowed for transmission of the incident beam and the exit of fluorescence X-rays from the sample to the detector.

The redox conditions of the system at various temperatures were buffered by the reaction $Re + O_2 \leftrightarrow ReO_2$ [36–39]. The appearance of rhenium oxide on the gasket surface indicates that partial oxidation of the Re metal gasket occurred in these experiments (Figure 5).

3.3. Synchrotron X-Ray Fluorescence Analysis. Synchrotron X-ray fluorescence (SXRF) spectra were collected using the X-ray microprobe at beamline 20-ID at the Advanced Photon Source (APS), Argonne National Laboratory. X-ray fluorescence spectra were collected using a four-element Vortex

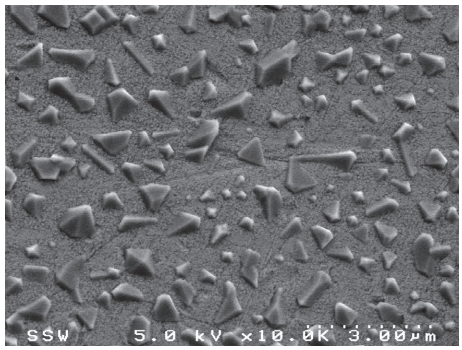

Figure 5: SEM image of ReO_2 crystals on the rhenium gasket surface after following the experiment.

Table 2: Measured Mo concentrations in standard solutions.

Standard (ppm)	Measured concentration (ppm)
10	31
50	75
100	141
500	543
1000	977
2500	2500

detector positioned horizontally at 90° to the incident X-ray beam. The energy of the incident X-rays was 23.2 keV and the beam flux was 1×10^{11} photons/second. The precise positioning of the X-ray beam through the sample chamber was facilitated by the visible fluorescence of the beam in the diamond anvil (Figure 3(b)).

Standard solutions having Mo concentrations of 10, 50, 100, 500, 1000, and 2500 ppm were used to derive a calibration curve. The solutions were prepared by diluting 10000 ppm (GFS Chemical) or 1000 ppm (Fluka Analytical) stock solutions with deionized water. An average of seven spectra was collected from each standard solution in the HDAC. The integration time for each spectrum was 60 s. PyMCA spectral analysis software [40] was used to analyze all SXRF spectra.

Table 2 gives the measured Mo concentrations for the standard solutions and Figure 6 shows the calibration curve determined by linear regression of the standard solution data [41].

3.4. Experimental Method. Deionized water, a small fragment of synthetic MoO_2, and an air bubble were sealed in the sample chamber in the HDAC (Figure 7(a)). The gasket was conditioned by repeated heating and cooling until the observed liquid-vapour homogenization temperature (T_H) was constant.

Spectra were collected from the fluid in 30-minute intervals for up to 4 hours. The HDAC was held at 400, 500, 600, 700, and 800°C for at least 30 minutes before the first spectrum was collected.

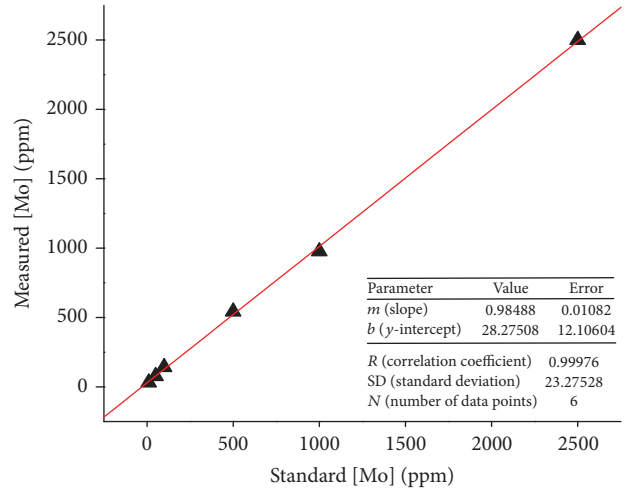

Figure 6: Calibration curve derived from measured Mo concentrations in standard solution.

Table 3: The measured concentration of Mo in solution at different temperatures and pressures.

Temperature (°C)	Pressure (MPa)	Concentration (ppm)
400	95	bdl*
500	193	bdl*
600	292	44 (±26)
700	387	67 (±26)
700	387	117 (±26)
800	479	658 (±43)

*bdl: below detection limit.

It was noted during trial runs that prolonged exposure to the X-ray beam at high temperatures resulted in the precipitation of a Mo-rich solid from the fluid at some point along the beam path (Figure 7(b)). In order to eliminate this effect, spectrum acquisition was limited to 60 s intervals.

Two-dimensional Mo $K\alpha$ elemental maps of the sample chamber were made at each pressure and temperature condition to correct for any changes in the position of the HDAC due to thermal expansion and to make sure that no Mo-bearing solids, formed by beam-induced radiolysis, were present.

4. Data Treatment and Results

The density of the fluid (684 kg/m^3) was calculated from the observed liquid-vapour homogenization temperature (313°C). Table 3 gives the pressure and temperature condition for each SXRF measurement.

The concentration of dissolved Mo in the fluid at each temperature and pressure condition was determined using the linear regression parameters of the calibration curve (Table 3). Examples of SXRF spectra obtained for three different molybdenum standards are shown in Figure 8. The

(a) (b)

Figure 7: View of the sample chamber in the HDAC at 23°C (a) and 600°C (b). Note the presence of a vapour bubble at room temperature and a small opaque phase (red arrow) in the center of sample chamber at 600°C.

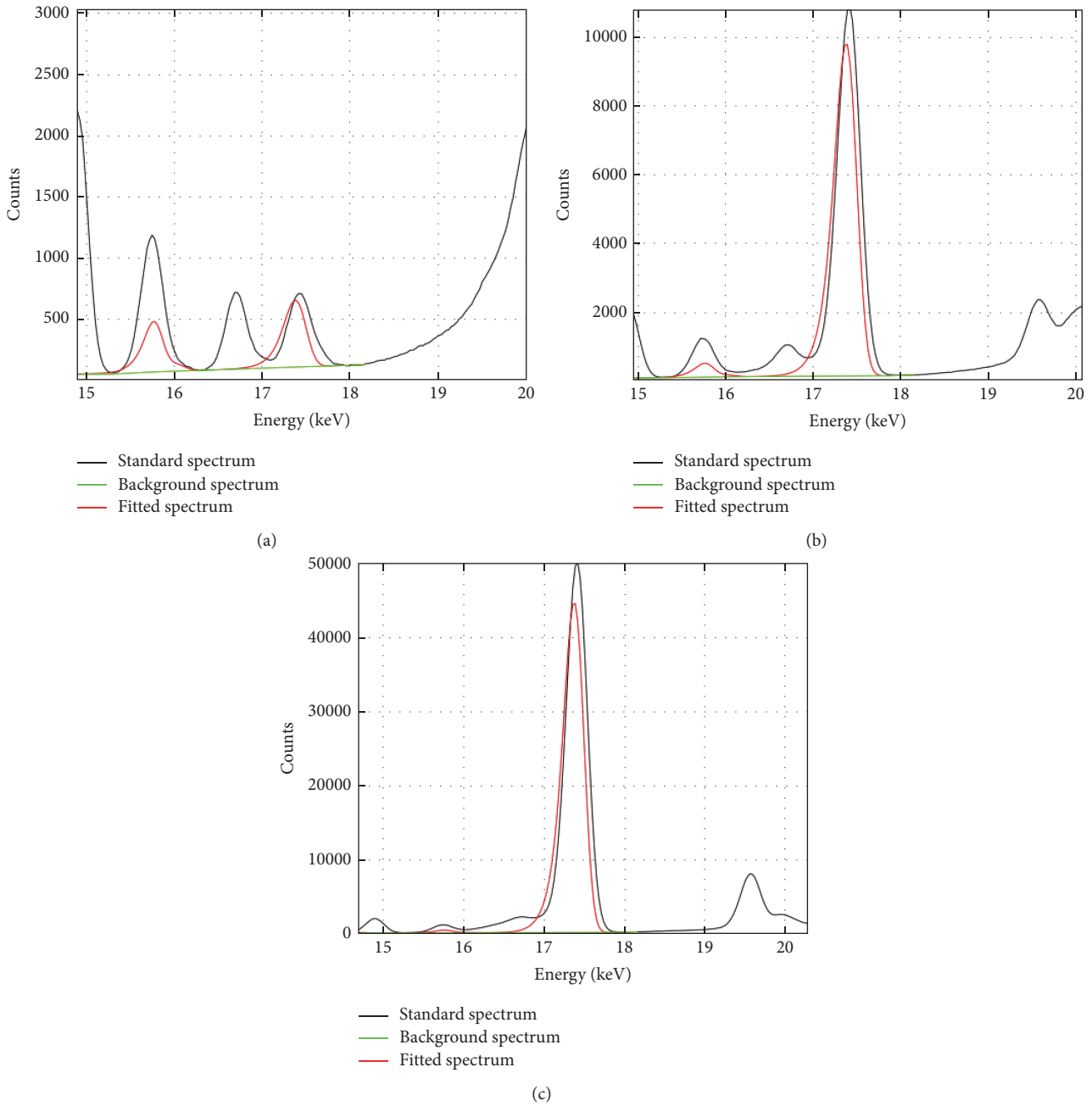

Figure 8: X-ray fluorescence spectra obtained from Mo standards (a) 10 ppm, (b) 500 ppm, and (c) 2500 ppm.

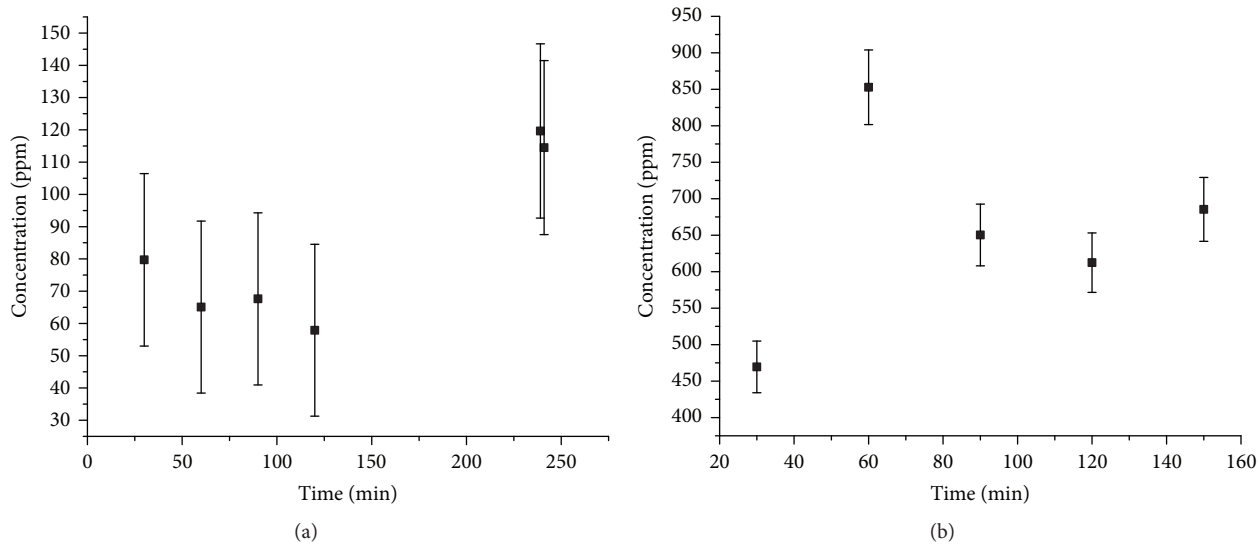

Figure 9: Variation of Mo concentration determined from XRF spectra collected at different time intervals at (a) 700°C and (b) 800°C.

uncertainty of the measured concentration was calculated using

$$S_x = \frac{S_y}{|m|}\sqrt{\frac{1}{k} + \frac{S_m^2 x^2}{S_y} + \left(\frac{S_b}{S_y}\right)^2 - \frac{2xS_m^2\overline{x}}{S_y^2}}, \quad (1)$$

where S_x is the uncertainty in x, $|m|$ is the absolute value of the slope, S_y is the standard deviation of the measured values of y, b is the intercept value, S_b is the intercept error or the estimate of standard deviation of the intercept, S_m is the slope error or the estimate of standard deviation of the slope, $\overline{x}$ is the arithmetic mean of used standard concentrations, and k is the number of replicate measurements of the unknown [41].

A minimum detection limit (MDL) of 0.5 to 3.0 ppm Mo was calculated from $3c\sqrt{I_b}/I_p$, where c is the standard concentration, I_b is the background intensity, and I_p is the peak intensity [42, 43].

Kudrin [8] examined the dissolution kinetics for MoO_2 in pure water and showed that equilibrium was attained after about 2 hours at 450°C and $\log fO_2 = -25.1$. The HDAC in our study was held between 2 and 4 hours prior to SXRF analysis. Figure 9 shows that at 700°C the Mo concentration varies from 70 ± 26 ppm in the first 2 hours and increases to 117±27 ppm after four hours. At 800°C, the Mo concentration is 686 (±43) ppm after 2.5 hours.

5. Discussion

Previous studies have shown that the molybdenum oxide solubility is effected to different degrees by solution composition, temperature, pressure, pH, and oxygen fugacity. Our analyses show that there is an exponential increase in solubility at temperatures above 500°C (Figure 10) which indicates that pure water could transport significant concentrations of Mo at magmatic temperatures.

Ulrich and Mavrogenes [4] presented solubility data for molybdenum in H_2O at temperatures between 500 and 800°C. In all of their experiments MoO_3 was reduced to MoO_2 and Mo was oxidized to MoO_2. The presence of a small opaque phase, interpreted to be MoO_2, present in some of their synthetic fluid inclusions indicates that MoO_2 precipitated from the solution at high temperatures prior to microcrack healing. If equilibrium was attained before fluid entrapment, then the concentration of Mo in that fluid should reflect the solubility of MoO_2. However, the solubility reported by Ulrich and Mavrogenes (2008) at 800°C and 200 MPa (i.e., 0.8 wt%) is more than an order of magnitude higher than the solubility reported in the present study. This discrepancy may be due in part to differences in the pressure conditions used in the different experiments or because the synthetic inclusions represent samples of fluid that equilibrated with the highly soluble MoO_3 used as starting material in the experiments of Ulrich and Mavrogenes (2008). The reduction of the fluid at high temperatures may have resulted in the precipitation of MoO_2 during closure and necking of the fluid-filled microcracks in quartz.

5.1. Molybdenum in Intrusion-Related Hydrothermal Systems. Many ore deposits of molybdenum form in high temperature intrusion-related hydrothermal systems. Fluid inclusion studies suggest that Mo deposition usually occurs at temperatures between 450 and about 700°C and pressures between 100 and 170 MPa [44–51]. Furthermore, Mo is thought to be transported by low to intermediate density, supercritical aqueous fluids [52–56] as mononuclear hydroxy complexes [57–61]. Although Mo is usually transported in the hexavalent state it is also transported in a lower valence state ($^+4$) under more reducing conditions [8, 62].

The temperature-redox conditions for porphyry Mo deposits are shown in Figure 11 [63, 64]. At these ore-forming conditions, MoO_2 rather than MoO_3 is the stable oxide [4, 7, 11, 12]. Fluid inclusion studies of porphyry Mo deposits indicate that low salinity fluids play an important role in Mo transport [65–70]. Candela and Holland [58] concluded that

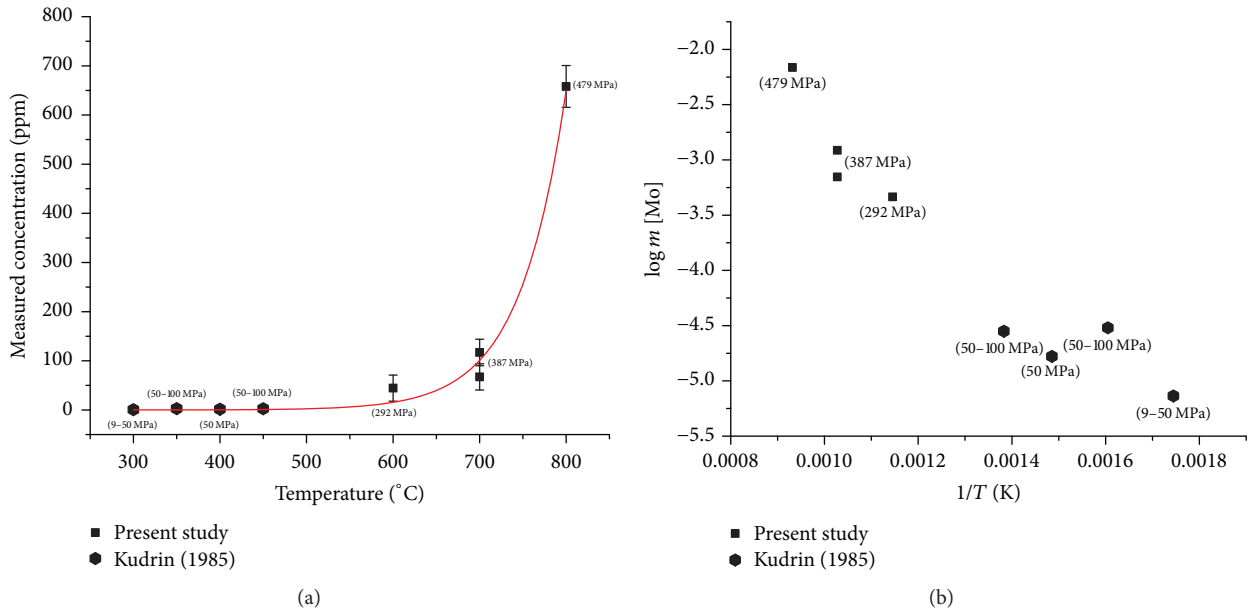

FIGURE 10: Solubility MoO_2 solubility in pure water as a function of temperature. The pressure condition for each measurement is shown on each plot.

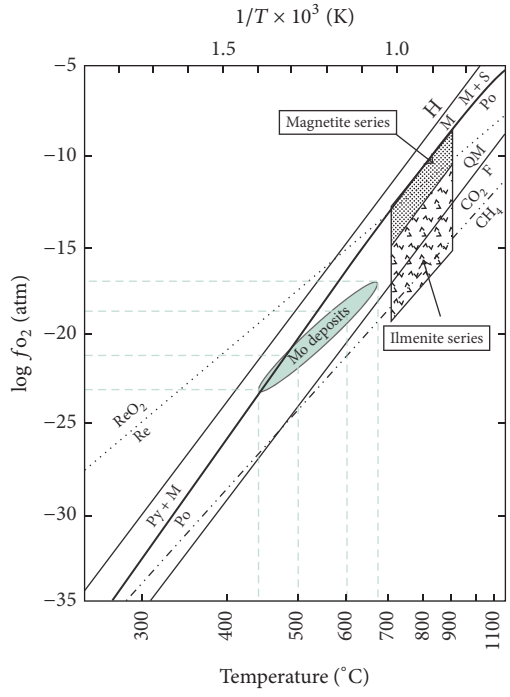

FIGURE 11: Temperature and fO_2 conditions for porphyry Mo deposits (modified after Ishihara et al. 2006). Re-ReO_2 buffer curve is shown.

in magmatic systems Mo partitioning is independent of the chlorine content of magmas and associated aqueous phases. Zajacz et al. [54] studied the effect of fluid chlorinity as a parameter on fluid/melt partitioning. They distinguished a group of elements (As, Mo, Cu, Sb, Bi, and B) displaying a distinct negative correlation with the chlorinity of the fluid, which suggests transport as non-chloride (i.e., hydroxy) complexes. Of these elements, Mo, As, Sb, and B are known to occur as hydroxy complexes in hydrothermal fluids [71–74]. Fluorine is not an important ligand involved in the hydrothermal transport of Mo in granite-related systems [58, 61, 75]. Some studies have demonstrated the importance of chloride complexing for Mo partitioning [4, 76]. Ulrich and Mavrogenes (2008) suggested a correlation between the solubility of Mo oxides and the chloride content in the fluid. Tattitch and Blundy (2017) have shown that fluid-melt Mo partition coefficient increases with the increasing salinity and a mono-chloride complex controls Mo partitioning. The results presented here may explain why low salinity fluid inclusions prevail in some Mo ore deposits. The presence of sulfur in such systems would result in the precipitation of molybdenite [10, 77–79].

5.2. Relevance of MoO_2 Solubility to Supercritical-Water-Cooled Reactor (SCWR). As discussed above, Generation-IV SCWR is designed to function at temperatures up to 625°C and at pressures ranging from 25 to 30 MPa. The successful deployment and long term operation of these SCWR depends on the durability of the materials in the presence of water under conditions of extreme temperature, pressure, and radiation [15, 18–20]. Mo-bearing alloys are among the candidate materials considered in the construction of SCWR. Previous experiments have shown that a significant amount of Mo from the walls of Hastelloy C and Alloy 625 autoclaves may be dissolved in pure water at 450°C after 280 hours [15]. Molybdenum oxides may form in the passivation layer of steel alloys [80–87] and dissolution of these oxides could result in contamination and degradation of the reactor performance by creating thermal barriers on heat transfer surfaces.

The next generation of supercritical water reactors are expected to operate at even higher pressures and temperatures [17]. The data shown in this study indicate that partially dissolution of a Mo-bearing passivation layer in a SCWR may affect water chemistry and the efficiency of the reactor. This example underscores the need to compile a more comprehensive oxide solubility database that can be used to predict supercritical water chemistry. To achieve this goal, we recommend that in situ SXRF solubility measurements be employed to experimentally evaluate the durability of candidate alloys under conditions of extreme temperature and pressure.

6. Conclusions

In situ synchrotron X-ray fluorescence analysis of aqueous fluids in a modified hydrothermal diamond anvil cell was used to determine the solubility of synthetic MoO_2 in pure water up to 800°C and 480 MPa. The results show an exponential increase in solubility at temperatures above 600°C to a maximum concentration of 658 ± 43 ppm Mo at 800°C and 480 MPa. The results on the MoO_2-H_2O system provide insights into Mo transport in pure water and in low salinity, high temperature aqueous solutions involved in ore-forming systems. The data are also relevant to understanding Mo transport in supercritical-water-cooled reactors and demonstrate the potential of in situ SXRF for further solubility studies of sparingly soluble oxide minerals under conditions of extreme temperature and pressure.

Conflicts of Interest

The authors declare that there are no conflicts of interest regarding the publication of this article.

Acknowledgments

This research used resources of the Advanced Photon Source (APS), an Office of Science User Facility operated for the US Department of Energy (DOE) Office of Science by Argonne National Laboratory, and was supported by the US DOE under Contract no. DE-AC02-06CH11357 and the Canadian Light Source and its funding partners. The authors thank Dr. Steve Heald for his assistance with our experiment at sector 20 of the APS. We acknowledge support from the GEN-IV program. Funding to the Canada Gen-IV National Program was provided by Natural Resources Canada through the Office of Energy Research and Development, Atomic Energy of Canada Limited, and Natural Sciences and Engineering Research Council of Canada. Pritam Saha acknowledges the receipt of support from the CLS Graduate and Post-Doctoral Student Travel Support Program and Nova Scotia Graduate Scholarship.

References

[1] G. F. Ivanova, N. I. Lavkina, L. A. Nesterova, and A. P. Zhudikova, "Equilibrium in the MoO3-H2O system at 25–300°C," *Geochemistry International*, vol. 12, pp. 163–176, 1975.

[2] Q. Gong, C. Yu, K. Cen, and Y. Wang, "Experimental determination of MoO3 and WO3 solubilities in supercritical fluids," *Acta Petrologica Sinica*, vol. 21, no. 1, pp. 240–244, 2005.

[3] K. U. Rempel, A. A. Migdisov, and A. E. Williams-Jones, "The solubility and speciation of molybdenum in water vapour at elevated temperatures and pressures: Implications for ore genesis," *Geochimica et Cosmochimica Acta*, vol. 70, no. 3, pp. 687–696, 2006.

[4] T. Ulrich and J. Mavrogenes, "An experimental study of the solubility of molybdenum in H2O and KCl-H2O solutions from 500 ∘C to 800 ∘C, and 150 to 300 MPa," *Geochimica et Cosmochimica Acta*, vol. 72, no. 9, pp. 2316–2330, 2008.

[5] P. R. Meredith, A. J. Anderson, and R. A. Mayanovic, "An in-situ investigation of the solubility of molybdenum trioxide in oxygenated water at supercritical conditions," in *Proceedings of the 5th International Symposium on Supercritical Water-Cooled Reactors*, 2011.

[6] T. P. Dadze, G. A. Kashirtseva, M. P. Novikov, A. V. Plyasunov, and Y. B. Shapovalov, "The solubility of MoO3 in aqueous solutions of HClO4 at T = 300°C and P = 100 bar by experimental data," *Doklady Earth Sciences*, vol. 456, no. 1, pp. 548-549, 2014.

[7] N. C. Hurtig and A. E. Williams-Jones, "An experimental study of the solubility of MoO3 in aqueous vapour and low to intermediate density supercritical fluids," *Geochimica et Cosmochimica Acta*, vol. 136, pp. 169–193, 2014.

[8] A. V. Kudrin, "The solubility of tugarinovite MoO2 in aqueous solutions at elevated temperatures.," *Geochemistry International*, vol. 22, no. 9, pp. 126–138, 1985.

[9] A. V. Kudrin, "Behavior of Mo in aqueous NaCl and KCl solutions at 300-450∘C," *Geochemistry International*, vol. 26, no. 8, pp. 87–99, 1989.

[10] X. Cao, *Solubility of Molybdenite and The Transport of Molybdenum in Hydrothermal Solutions*, Iowa State University, Ames, Iowa, USA, 1989.

[11] G. Solferino and A. J. Anderson, "Thermal reduction of molybdite and hematite in water and hydrogen peroxide-bearing solutions: Insights on redox conditions in Hydrothermal Diamond Anvil Cell (HDAC) experiments," *Chemical Geology*, vol. 322-323, pp. 215–222, 2012.

[12] P. A. Spevack and S. McIntyre, "Reactivity and stability of sulphided thin films of molybdenum to dry air," *Applied Catalysis*, vol. 64, no. C, pp. 191–207, 1990.

[13] H. N. Lander, "Energy related uses of molybdenum," *Molybdenum in the Environment*, vol. 2, p. 773, 1977.

[14] R. B. Ross, *Metallic materials specification handbook*, Springer Science & Business Media, 2013.

[15] D. Guzonas, P. Tremaine, and J.-P. Jay-Gerin, "Chemistry control challenges in a supercritical water-cooled reactor," *Power Plant Chemistry*, vol. 11, no. 5, pp. 284–291, 2008.

[16] D. Guzonas and R. Novotny, "Supercritical water-cooled reactor materials - Summary of research and open issues," *Progress in Nuclear Energy*, vol. 77, pp. 361–372, 2014.

[17] U. S. DoE, "A technology roadmap for generation IV nuclear energy systems," in *Proceedings of the Nuclear Energy Research Advisory Committee and the Generation IV International Forum*, 2002.

[18] G. P. Gu, W. Zheng, and D. Guzonas, "Corrosion database for SCWR development," in *Proceedings of the 2nd Canada-China Joint Workshop on Supercritical-Water-Cooled Reactors*, 2010.

[19] S. Baindur, "Materials challenges for the supercritical water-cooled reactor (SCWR)," *Bulletin of the Canadian Nuclear Society*, vol. 29, no. 1, pp. 32–38, 2008.

[20] D. F. Torgerson, B. A. Shalaby, and S. Pang, "CANDU technology for Generation III+ and IV reactors," *Nuclear Engineering and Design*, vol. 236, no. 14-16, pp. 1565–1572, 2006.

[21] T. R. Allen, Y. Chen, L. Tan, X. Ren, K. Sridharan, and S. Ukai, "Corrosion of candidate materials for supercritical water-cooled reactors," in *Proceedings of the 12th International Conference on Environmental Degradation of Materials in Nuclear Power Systems-Water Reactors*, pp. 1397–1407, August 2005.

[22] W. A. Bassett, A. H. Shen, M. Bucknum, and I.-M. Chou, "A new diamond anvil cell for hydrothermal studies to 2.5 GPa and from –190 to 1200°C," *Review of Scientific Instruments*, vol. 64, no. 8, pp. 2340–2345, 1993.

[23] A. Verlaguet, F. Brunet, B. Goffá, and W. M. Murphy, "Experimental study and modeling of fluid reaction paths in the quartz-kyanite ± muscovite-water system at 0.7 GPa in the 350–550°C range: Implications for Al selective transfer during metamorphism," *Geochimica et Cosmochimica Acta*, vol. 70, no. 7, pp. 1772–1788, 2006.

[24] H. Bureau and M. Burchard, "In situ characterization of geological materials at high pressure and temperature: Techniques and observations - A special session at the 2005 AGU Fall Meeting, San Francisco, USA," *High Pressure Research*, vol. 26, no. 3, pp. 233-234, 2006.

[25] A. Verlaguet and F. Brunet, "Effect of incongruent dissolution on mineral solubility data derived from quench experiments," *European Journal of Mineralogy*, vol. 19, no. 6, pp. 783–789, 2007.

[26] T. Fockenberg, M. Burchard, and W. V. Maresch, "The solubility of natural grossular-rich garnet in pure water at high pressures and temperatures," *European Journal of Mineralogy*, vol. 20, no. 5, pp. 845–855, 2008.

[27] J. Moosburger-Will, M. Krispin, M. Klemm, and S. Horn, "LEED and STM studies of the stability of the MoO2(100) surface," *Surface Science*, vol. 605, no. 15-16, pp. 1442–1448, 2011.

[28] T. Hörlin, T. Niklewski, and M. Nygren, "Magnetic, electrical and thermal studies on the V1-xMoxO2 system," *Materials Research Bulletin*, vol. 8, no. 2, pp. 179–189, 1973.

[29] R. Jenkins, T. G. Fawcett, D. K. Smith, J. W. Visser, M. C. Morris, and L. K. Frevel, "JCPDS—International Centre for Diffraction Data Sample Preparation Methods in X-Ray Powder Diffraction," *Powder Diffraction*, vol. 1, no. 2, pp. 51–63, 1986.

[30] P. A. Spevack and N. S. McIntyre, "Thermal reduction of MoO3," *The Journal of Physical Chemistry C*, vol. 96, no. 22, pp. 9029–9035, 1992.

[31] E. Payen, J. Grimblot, and S. Kasztelan, "Study of oxidic and reduced alumina-supported molybdate and heptamolybdate species by in situ laser Raman spectroscopy," *The Journal of Physical Chemistry C*, vol. 91, no. 27, pp. 6642–6648, 1987.

[32] J. G. Grasselli, M. K. Snavely, and B. J. Bulkin, "Applications of Raman spectroscopy," *Physics Reports*, vol. 65, no. 4, pp. 231–344, 1980.

[33] A. H. Shen, W. A. Bassett, and I. Chou, "Hydrothermal Studies in a Diamond Anvil Cell: Pressure Determination Using the Equation of State of H," in *High-Pressure Research: Application to Earth and Planetary Sciences*, Geophysical Monograph Series, pp. 61–68, American Geophysical Union, Washington, Wash, USA, 1992.

[34] A. H. Shen, I. M. Chou, and W. A. Bassett, "Experimental determination of isochores of H2O in a diamond-anvil cell up to 1200 MPa and 860°C with preliminary results in the NaCl-H2O system," in *Proceedings of the 4th International Symposium on Hydrothermal Reactions*, pp. 235–239, Nancy, France, 1993.

[35] W. Wagner and A. Pruß, "The IAPWS formulation 1995 for the thermodynamic properties of ordinary water substance for general and scientific use," *Journal of Physical and Chemical Reference Data*, vol. 31, no. 2, pp. 387–535, 2002.

[36] A. Audétat and H. Keppler, "Solubility of rutile in subduction zone fluids, as determined by experiments in the hydrothermal diamond anvil cell," *Earth and Planetary Science Letters*, vol. 232, no. 3-4, pp. 393–402, 2005.

[37] R. S. Chellappa, M. Somayazulu, and R. J. Hemley, "Rhenium reactivity in H2O-O2 supercritical mixtures at high pressures," *High Pressure Research*, vol. 29, no. 4, pp. 792–799, 2009.

[38] I.-M. Chou and A. J. Anderson, "Diamond dissolution and the production of methane and other carbon-bearing species in hydrothermal diamond-anvil cells," *Geochimica et Cosmochimica Acta*, vol. 73, no. 20, pp. 6360–6366, 2009.

[39] M. Marocchi, H. Bureau, G. Fiquet, and F. Guyot, "In-situ monitoring of the formation of carbon compounds during the dissolution of iron(II) carbonate (siderite)," *Chemical Geology*, vol. 290, no. 3-4, pp. 145–155, 2011.

[40] V. A. Solé, E. Papillon, M. Cotte, P. Walter, and J. Susini, "A multiplatform code for the analysis of energy-dispersive X-ray fluorescence spectra," *Spectrochimica Acta Part B: Atomic Spectroscopy*, vol. 62, no. 1, pp. 63–68, 2007.

[41] D. C. Harris, "Calibration methods," in *Modified Hydrothermal Diamond Anvil Cells for XAFS Analyses of Elements with Low Energy Absorption Edges in Aqueous Solutions at Sub- and Supercritical Conditions*, vol. 5, pp. 85–88, New York, NY, USA, 2010.

[42] M. Haller and A. Knöchel, "X-ray fluorescence analysis using synchrotron radiation (SYXRF)," *Journal of Trace and Microprobe Techniques*, vol. 14, no. 3, pp. 461–488, 1996.

[43] P. Wobrauschek, C. Streli, and E. Selin Lindgren, *Energy dispersive, X-ray fluorescence analysis*, John Wiley & Sons, Ltd, Chichester, UK, 2006.

[44] E. Roedder, "Fluid inclusion studies on the porphyry-type ore deposits at Bingham, Utah, Butte, Montana, and Climax, Colorado," *Economic Geology*, vol. 66, no. 1, pp. 98–118, 1971.

[45] W. E. Hall, I. Friedman, and J. T. Nash, "Fluid inclusion and light stable isotope study of the climax molybdenum deposits, Colorado," *Economic Geology*, vol. 69, no. 6, pp. 884–901, 1974.

[46] K. L. Shelton, C. S. So, D. M. Rye, and M. E. Park, "Geologic, sulfur isotope, and fluid inclusion studies of the Sannae W-Mo mine, Republic of Korea: comparison of sulfur isotope systematics in Korean W deposits.," *Economic Geology*, vol. 81, no. 2, pp. 430–446, 1986.

[47] K. L. Shelton, R. P. Taylor, and Chil-Sup So, "Stable isotope studies of the Dae Hwa tungsten- molybdenum mine, Republic of Korea: evidence of progressive meteoric water interaction in a tungsten-bearing hydrothermal system.," *Economic Geology*, vol. 82, no. 2, pp. 471–481, 1987.

[48] K. L. Shelton, "Composition and origin of ore-forming fluids in a carbonate- hosted porphyry copper and skarn deposit: a fluid inclusion and stable isotope study of Mines Gaspe, Quebec.," *Economic Geology*, vol. 78, no. 3, pp. 387–421, 1983.

[49] C. S. So, D. M. Rye, and K. L. Shelton, "Carbon, hydrogen, oxygen, and sulfur isotope and fluid inclusion study of the Weolag tungsten-molybdenum deposit, Republic of Korea: fluid histories of metamorphic and ore-forming events.," *Economic Geology*, vol. 78, no. 8, pp. 1551–1573, 1983.

[50] J. R. Lang and C. J. Eastoe, "Relationships between a porphyry Cu-Mo deposit, base and precious metal veins, and Laramide

intrusions, Mineral Park, Arizona," *Economic Geology*, vol. 83, no. 3, pp. 551–567, 1988.

[51] G. F. Ivanovo, Z. M. Motorina, and V. B. Naumov, "Formation features of the mineral associations of the yugodzyr' molybdenum-tungsten deposit (Mongolia)," *International Geology Review*, vol. 20, no. 7, pp. 855–863, 1978.

[52] C. W. Burnham, "Magmas and hydrothermal fluids," in *Geochemistry of hydrothermal ore deposits*, H. L. Barnes, Ed., pp. 71–136, 1979.

[53] C. J. Eastoe, "Physics and chemistry of the hydrothermal system at the Panguna porphyry copper deposit, Bougainville, Papua New Guinea.," *Economic Geology*, vol. 77, no. 1, pp. 127–153, 1982.

[54] Z. Zajacz, W. E. Halter, T. Pettke, and M. Guillong, "Determination of fluid/melt partition coefficients by LA-ICPMS analysis of co-existing fluid and silicate melt inclusions: Controls on element partitioning," *Geochimica et Cosmochimica Acta*, vol. 72, no. 8, pp. 2169–2197, 2008.

[55] J. H. Seo, M. Guillong, and C. A. Heinrich, "Separation of molybdenum and copper in porphyry deposits: The roles of sulfur, redox, and pH in ore mineral deposition at bingham canyon," *Economic Geology*, vol. 107, no. 2, pp. 333–356, 2012.

[56] L. Lerchbaumer and A. Audétat, "High Cu concentrations in vapor-type fluid inclusions: An artifact?" *Geochimica et Cosmochimica Acta*, vol. 88, pp. 255–274, 2012.

[57] R. Kolonin, Y. Laptev, and P. Biteikina, "Formation condition of molybdenite and powellite in hydrothermal solutions," *Experimental Studies in Mineralogy*, pp. 27–33, 1975.

[58] P. A. Candela and H. D. Holland, "A mass transfer model for copper and molybdenum in magmatic hydrothermal systems: the origin of porphyry-type ore deposits.," *Economic Geology*, vol. 81, no. 1, pp. 1–19, 1986.

[59] S. Arnórsson and G. Ívarsson, "Molybdenum in icelandic geothermal waters," *Contributions to Mineralogy and Petrology*, vol. 90, no. 2-3, pp. 179–189, 1985.

[60] M. Štemprok, "Solubility of tin, tungsten and molybdenum oxides in felsic magmas," *Mineralium Deposita*, vol. 25, no. 3, pp. 205–212, 1990.

[61] H. Keppler and P. J. Wyllie, "Partitioning of Cu, Sn, Mo, W, U, and Th between melt and aqueous fluid in the systems haplogranite-H2O-HCl and haplogranite-H2O-HF," *Contributions to Mineralogy and Petrology*, vol. 109, no. 2, pp. 139–150, 1991.

[62] L. Robb, *Introduction to Ore-Forming Processes*, John Wiley & Sons, 2013.

[63] H. Ohmoto and M. B. Goldhaber, "Sulfur and carbon isotopes," *Geochemistry of Hydrothermal Ore Deposits*, vol. 3, pp. 517–611, 1997.

[64] S. Ishihara, H. Ohmoto, C. R. Anhaeusser, A. Imai, and L. J. Robb, "Discovery of the oldest oxic granitoids in the Kaapvaal Craton and its implications for the redox evolution of early Earth," *Geological Society of America Memoirs*, vol. 198, pp. 67–80, 2006.

[65] S. A. Roberts, *Early hydrothermal alteration and mineralization in the Butte district, Montana*, Harvard University, 1975.

[66] W. H. White, A. A. Bookstrom, R. J. Kamilli et al., "Character and origin of Climax-type molybdenum deposits," *Economic Geology*, vol. 75, pp. 270–316, 1981.

[67] B. G. Rusk, M. H. Reed, J. H. Dilles, L. M. Klemm, and C. A. Heinrich, "Compositions of magmatic hydrothermal fluids determined by LA-ICP-MS of fluid inclusions from the porphyry copper-molybdenum deposit at Butte, MT," *Chemical Geology*, vol. 210, no. 1-4, pp. 173–199, 2004.

[68] C. A. Heinrich, "The physical and chemical evolution of low-salinity magmatic fluids at the porphyry to epithermal transition: a thermodynamic study," *Mineralium Deposita*, vol. 39, no. 8, pp. 864–889, 2005.

[69] L. M. Klemm, T. Pettke, C. A. Heinrich, and E. Campos, "Hydrothermal evolution of the El Teniente deposit, Chile: Porphyry Cu-Mo ore deposition from low-salinity magmatic fluids," *Economic Geology*, vol. 102, no. 6, pp. 1021–1045, 2007.

[70] B. G. Rusk, M. H. Reed, and J. H. Dilles, "Fluid inclusion evidente for magmatic-hydrothermal fluid evolution in the porphyry copper-molybdenum deposit at Butte, Montana," *Economic Geology*, vol. 103, no. 2, pp. 307–334, 2008.

[71] A. V. Zotov, N. D. Shikina, and N. N. Akinfiev, "Thermodynamic properties of the Sb(III) hydroxide complex Sb(OH)3(aq) at hydrothermal conditions," *Geochimica et Cosmochimica Acta*, vol. 67, no. 10, pp. 1821–1836, 2003.

[72] D. Testemale, J.-L. Hazemann, G. S. Pokrovski et al., "Structural and electronic evolution of the As(OH)3 molecule in high temperature aqueous solutions: An x-ray absorption investigation," *The Journal of Chemical Physics*, vol. 121, no. 18, pp. 8973–8982, 2004.

[73] C. Schmidt, R. Thomas, and W. Heinrich, "Boron speciation in aqueous fluids at 22 to 600∘C and 0.1 MPa to 2 GPa," *Geochimica et Cosmochimica Acta*, vol. 69, no. 2, pp. 275–281, 2005.

[74] G. S. Pokrovski, A. Y. Borisova, J. Roux et al., "Antimony speciation in saline hydrothermal fluids: A combined X-ray absorption fine structure spectroscopy and solubility study," *Geochimica et Cosmochimica Acta*, vol. 70, no. 16, pp. 4196–4214, 2006.

[75] D. R. Lentz and K. Suzuki, "A low F pegmatite-related Mo skarn from the Southwestern Grenville Province Ontario, Canada: Phase equilibria and petrogenetic implications," *Economic Geology*, vol. 95, no. 6, pp. 1319–1337, 2000.

[76] B. C. Tattitch and J. D. Blundy, " Cu-Mo partitioning between felsic melts and saline-aqueous fluids as a function of ," *American Mineralogist*, vol. 102, no. 10, pp. 1987–2006, 2017.

[77] T. N. Tingle and P. M. Fenn, "Transport and concentration of molybdenum in granite molybdenite systems: effects of fluorine and sulfur.," *Geology*, vol. 12, no. 3, pp. 156–158, 1984.

[78] S. A. Wood, D. A. Crerar, and M. P. Borcsik, "Solubility of the assemblage pyrite-pyrrhotite-magnetite-sphalerite-galena-gold-stibnite-bismuthinite-argentite-molybdenite in H2O-NaCl-CO2 Solutions from 200° to 350°C," *Economic Geology*, vol. 82, no. 7, pp. 1864–1887, 1987.

[79] Y. Gu, *Theoretical and experimental studies of the hydrothermal geochemistry of molybdenum*, Monash University, 1993.

[80] C.-O. A. Olsson and S. E. Hornstrom, "An AES and XPS study of the high alloy austenitic stainless steel 254 SMO® tested in a ferric chloride solution," *Corrosion Science*, vol. 36, no. 1, pp. 141–151, 1994.

[81] C.-O. A. Olsson and D. Landolt, "Passive films on stainless steels—chemistry, structure and growth," *Electrochimica Acta*, vol. 48, no. 9, pp. 1093–1104, 2003.

[82] C.-O. A. Olsson, "The influence of nitrogen and molybdenum on passive films formed on the austenoferritic stainless steel 2205 studied by AES and XPS," *Corrosion Science*, vol. 37, no. 3, pp. 467–479, 1995.

[83] I. Olefjord, B. Brox, and U. Jelvestam, "Surface composition of stainless steels during anodic dissolution and passivation studied by ESCA," *Journal of The Electrochemical Society*, vol. 132, no. 12, pp. 2854–2861, 1985.

[84] L. L. Wikstrom and K. Nobe, "The Electrochemical Behavior of Molybdenum," *Journal of The Electrochemical Society*, vol. 116, no. 4, p. 525, 1969.

[85] E. De Vito and P. Marcus, "XPS study of passive films formed on molybdenum-implanted austenitic stainless steels," *Surface and Interface Analysis*, vol. 19, no. 1-12, pp. 403–408, 1992.

[86] T. H. Heumann and G. Hauck, "Zur frage der kinetik der molybdanauflosung in sauren elektrolyten," *Zeitschrift Fur Metallkunde*, vol. 56, p. 75, 1965.

[87] M. Konig and H. Gohr, "Zur passivitat des molybdans in wassriger losung," *Berichte Der Bunsen-gesellschaft Fur Physikalische Chemie*, vol. 67, pp. 837-838, 1963.